Path Tracking Control of a Steerable Catheter in Transcatheter Cardiology Interventions

Xiu Zhang[1], Aditya Sridhar[2], Xuan Thao Ha[2], Syed Zain Mehdi[2], Andrea Fortuna[1], Mattia Magro[1], Angela Peloso[1], Anna Bicchi[1], Mouloud Ourak[2], Andrea Aliverti[1], Emiliano Votta[1], Emmanuel Vander Poorten[2†], Elena De Momi[1†]

[1*]Department of Electronics, Information and Bioengineering, Politecnico di Milano, Milan, 20133, Italy.
[2]Department of Mechanical Engineering, KU Leuven, Leuven, 3001, Belgium.

Contributing authors: xiu.zhang@polimi.com; aditya.sridhar@kuleuven.be; xuanthao.ha@kuleuven.be; syedzain.mehdi@kuleuven.be; andrea.fortuna@polimi.com; mattia.magro@polimi.com; angela.peloso@polimi.com; anna.bicchi@polimi.com; mouloud.ourak@kuleuven.be; andrea.aliverti@polimi.com; emiliano.votta@polimi.com; emmanuel.vanderpoorten@kuleuven.be; elena.demomi@polimi.com;
[†]These authors contributed equally to this work.

Abstract

Purpose: Interventions targeting the heart allow for reducing trauma and hospitalization stays. In case of mitral valve repair, the cardiologist delivers a clip through the vessel into the heart chamber. However, precise manipulation of the catheter from a long distance outside the body while moving in a constrained space remains challenging.

Methods: We proposed a path tracking control framework that provides adequate motion commands to the robotic steerable catheter for autonomous navigation through vascular lumens. The proposed work implements a catheter kinematic model featuring nonholonomic constraints. Relying on the real-time measurements from an Electromagnetic sensor and a Fiber Bragg Grating sensor, a two-level feedback controller was designed to control the catheter.

Results: The proposed method was tested in a patient-specific vessel phantom. A median position error between the center line of the vessel and the catheter tip trajectory was found to be below **2** mm, with a maximum error below **3** mm. **Conclusion:** The preliminary in-vitro studies presented in this paper showed promising accuracy in autonomously controlling a steerable catheter for transcatheter cardiology interventions.

Keywords: Cardiac interventions, Catheter robot, Motion Control, EM sensor, FBG-based sensors

1 Introduction

Mitral regurgitation (MR) is a type of heart valve disease in which the valve between the Left Atrium (LA) and the left ventricle (LV) doesn't completely close, allowing blood to leak backward. MR increases the pressure in the pulmonary venous channel and the left atrial chamber, weakening the heart walls, causing shortness of breath, fatigue, and in chronic cases, heart failure. According to the report from WHO, 1.7 % of US adult population and 9.3 % of adults over the age of 75 suffer from MR. Moreover, the annual mortality rate is about 34 %. Open-chest surgery can provide immediate relief unlike medication, but 50 % of the MR patients are not recommended open-heart surgery due to their age and possibilities of post-operative complications [1].

Transcatheter mitral valve repair approaches are gaining popularity due to reduced invasiveness and shorter recovery time. Moreover, transcatheter approaches offer an alternative treatment for patients who cannot undergo open-chest surgery. With the Food and Drug Administration (FDA) approved MitraClip^{TM} (MC) device (Abbott Laboratories, IL), the cardiologist inserts a steerable catheter from the femoral vein, passing a sequence of narrow and rugged vessels to reach the Right Atrium (RA). From there, the LA is accessed through a puncture in the atrial septum (Fig. 1). After successfully accessing the LA, the operator inserts the delivery catheter through the sheath catheter to the mitral valve and implants the clip [2]. However, to visualize the catheter during the procedure, both patients and operators would be exposed to damaging radiation [3]. In addition, given the poor image quality and the lack of depth, there would be a high risk of embolization or perforation [4].

To address these challenges in maneuvering MC catheter, we proposed a control framework for a customized-built actuator to autonomously advance the steerable catheter in a continuous fashion along the pre-planned path. By providing the appropriate steering commands based on the catheter kinematic model, the tip of the catheter tracked the center line of the vessel to avoid intense contact between the acute catheter tip and the fragile vessel wall. To ensure precise steering, a feedback controller is implemented to control the tension on the tendon and reject the error of the steering angle in the joint space. Experiments were carried out in a vessel phantom to evaluate the performance of the system.

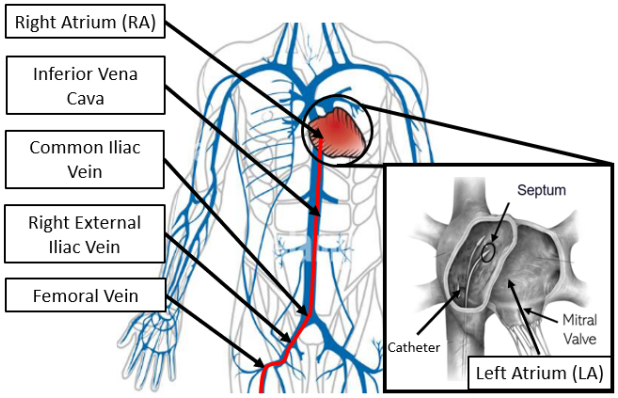

Fig. 1 Path of the transcatheter mitral valve repair procedure: The catheter passes through the femoral vein, right external iliac vein, common iliac vein, and inferior vena cava and arrives at the right atrium. From there, the mitral valve is reached by a transseptal puncture.

2 Related Work

Robotic technology has emerged as an important tool for catheters deployment. In 2011, CorPath 200 (Corindus Inc., United States) was introduced as the first robot-assisted system to control coronary guidewires and stents for coronary angioplasty procedure [5]. Subsequently, the Sensei Robotic Navigation System (Hansen Medical Inc., United States) was developed and evaluated for catheter ablation of atrial fibrillation [6] and ventricular arrhythmias [7]. The most recent Sensei X Robotic System (Hansen Medical Inc., United States) expands its application on collecting electrophysiological data inside the heart chambers [8]. Furthermore, researchers have developed catheter prototypes with haptic interfaces to enhance the safety of robot-assisted percutaneous coronary interventions (PCI) [9–11]. Despite successful clinical studies, robot-assisted PCI is only limited to a few clinics with skilled surgeons because of the steep learning curve and expensive hardware [12].

The adoption of task autonomy, where the surgeon supervises the procedure while the robot performs the task autonomously, could address this challenge [13–16]. Although robotic catheters are considered ideal for medical applications due to their particular structure, their compliance can pose difficulties in modeling and control. The robotic controller plays an important role in precisely navigating robots to complete the surgical procedure and avoid damaging surrounding tissues.

Open-loop control relies on model inversion to determine the appropriate actuation values for achieving the desired robot state. In the context of controlling robotic catheters, some researchers have proposed approaches based on specific kinematic models. [17–19]. Greigarn et al. introduce the pseudo-rigid-body (PRB) model on a robotic catheter by approximating the catheter as rigid links connected by flexible joints [20]. Bailly et al. proposed a differential model-based control scheme for a continuum robot [21]. Although these methods could control catheters in free space, it is still difficult to reach precise motion in realistic scenarios where catheters move

in a constrained environment (i.e. the vessels) where contact with the vessel wall is inevitable with open-loop approaches [22].

The data-driven approaches were investigated to overcome the challenges posed by the high complexity of continuum robot kinematics, Michael et al. proposed a model-less control method for controlling a tendon-driven continuum manipulator [23]. In addition, Di et al. introduced a deep-learning-based compliant motion controller for a robotic catheter [24]. However, the low compatibility rate of change in the environment and disturbances, as well as the complexity of learning approaches, may limit their application in medical scenarios where surgical instruments are single-use and patients have different anatomies [25].

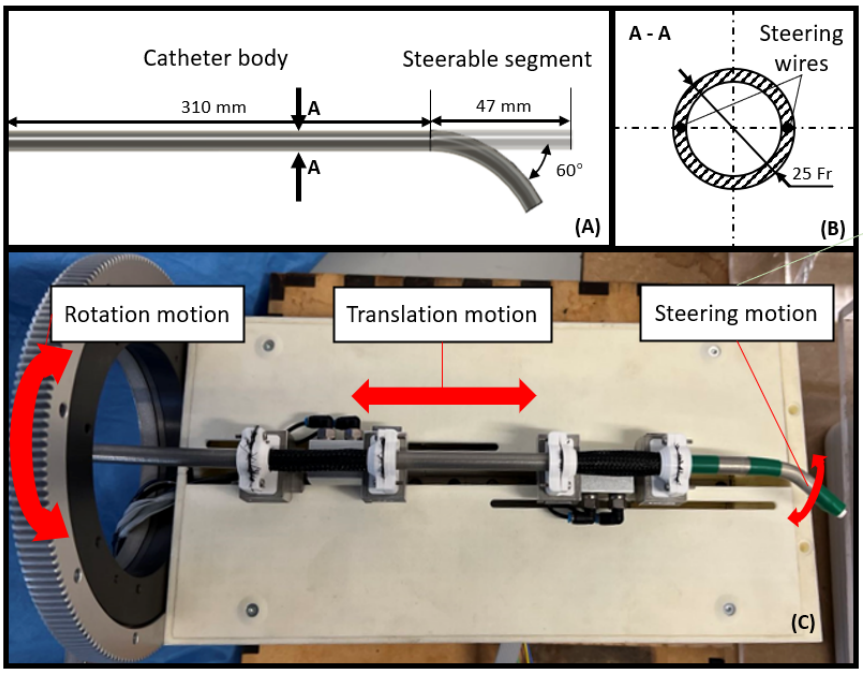

Fig. 2 Schematic of the catheter actuation system: (A) Top view of the steerable catheter shows a 310 mm long catheter body and a 47 mm long steerable segment with a maximum steering angle of 60°; (B) Cross-section view of the steerable catheter indicates the outer diameter of the catheter and the position of the steering wires; (C) The robotic system has three actuated DOFs in total, including the rotational motion, the translational motion, and the steering motion.

The development of pose-tracking techniques and shape sensors have demonstrated great potential to close the control loop of robotic catheters and compensate for the model inaccuracy. In particular, electromagnetic (EM) tracking techniques have been widely applied to track the robotic catheter within the human body [26, 27]. Loschak et al. developed a robotic ultrasound imaging catheter to control the position and orientation based on EM [28]. Omisore et al. proposed a robotic catheter with adaptive compensation of backlash with an EM sensor fixed at the tip of the catheter [29].

In addition, relying on the shape reconstruction from Fiber Bragg Grating (FBG) sensor, Sefati et al. designed an optimization-based control algorithm to position the continuum manipulators interacting with unknown obstacles [30].

3 Method

3.1 Steerable Catheter Kinematics

The tendon-driven steerable catheter is composed by a 310 mm long catheter body and a 47 mm long steerable segment at the distal tip side space(Fig. 2 (A)). The steerable segment is able to generate a 60° steering angle from the straight position. Two antagonistic steering wires travel along the length of the catheter body up to the tip of the 25 Fr steerable catheter to actuate the steerable segment (Fig. 2 (B)). Expect for the tendon-driven steering motion, based on our previous work [31], a catheter driver system with the sleeve-based grippers and the spur gear is used to generate decoupled 2 degrees of freedom (DOFs) (i.e., translation and rotation) (Fig. 2 (C)).

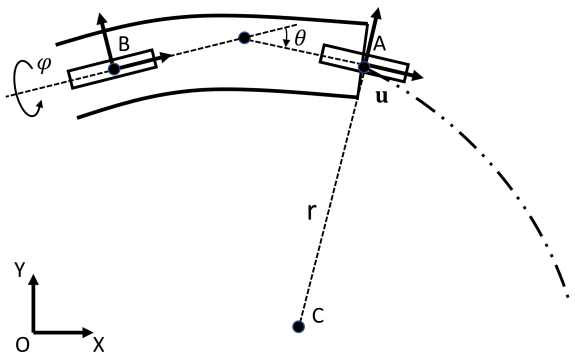

Fig. 3 Non-holonomic motion of the catheter modeled with a so-called "bicycle" model showing the steerable segment of the catheter showing the front and rear "wheels" at frame A and frame B of a bicycle model, including three DOFs: rotation angle φ, insertion speed $\mathbf{u}$, and in-plane steering angle θ.

Assuming that the translational motion and the rotational motion propagate ideally from the base through the catheter body to the tip. The distal steerable segment of the catheter can be modeled as a kinematic nonholonomic system [32], including all the three actuated DOFs. As shown in Fig. 3, the front wheel (A) of the bicycle is attached to the tip of the catheter, and the rear wheel (B) is located on the proximal end of the steerable segment. Generally speaking, advancing the catheter can be approximated as "cycling" forward at a speed, $\mathbf{u}$, and bending the catheter with an angle, θ, is like steering the front wheel of the bicycle. The combination of these two motions will generate a circular trajectory with a constant curvature radius, r, and a rotation center at point C. Furthermore, by rotating the catheter about its longitudinal axis with a rotation angle, φ, one can control the angle of the planar trajectory.

3.2 Control Strategy

This work combines two control strategies: 1) path tracking control, a high-level controller, is used to correct the motion of the steerable catheter when it deviates from the path; 2) feedback control, a low-level controller that drives the actuation system to reach a desired steering angle (Fig. 4).

3.2.1 High-level (Path tracking) controller

The path tracking controller is a nonlinear feedback controller which reduces the tracking error between the measured tip position $\mathbf{p}_{\mathrm{m}}$ and the closest point $\mathbf{p}_k$ on the desired path $\mathbf{p}_i[x_i, y_i, \gamma_i]$. The control law consists of two parts, which account for the orientation error, $e_\theta\,(t)$, and the distance offset error, $e_\delta\,(t)$, as shown in eq. (1) eq. (2), and eq. (3). These two terms are the steering control elements based on the "Stanly method" [33]. Within the control loop, $e_\theta\,(t)$ is intuitively aligning the orientation of the tip, $\gamma_m\,(t)$, to match the orientation of the desired path, $\gamma_k\,(t)$, and the second term adjusts the steering angle in (nonlinear) proportion to the distance error $e_d\,(t)$. In other words, it controls the steering angle, $\theta_d(t)$, such that the intended trajectory intersects the path at point $\mathbf{p}_d$ at the next time step $t+1$ (Fig. 5). Additionally, the contribution of $e_\theta\,(t)$ and $e_\delta\,(t)$ can be adjusted by tuning the orientation gain factor, k_θ, for adapting to different paths. The steering gain factor, k_d, determines the rate of convergence toward the path.

$$\theta_d\,(t) = k_\theta e_\theta\,(t) \pm e_\delta\,(t) \tag{1}$$

$$e_\theta\,(t) = \gamma_{\mathrm{m}}\,(t) - \gamma_k\,(t) \tag{2}$$

$$e_\delta\,(t) = f\left(e_d\,(t), \mathbf{u}\,(t)\right) = \arctan\left(\frac{k_d e_d\,(t)}{\|\mathbf{u}\,(t)\|}\right) \tag{3}$$

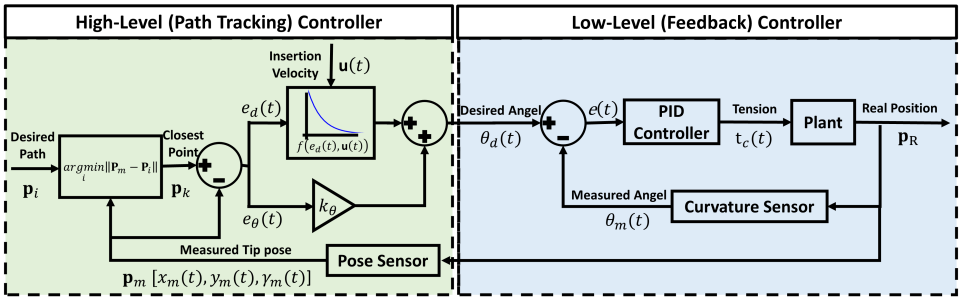

Fig. 4 Control framework: The high-level controller accepts the pre-operative desired path $\mathbf{p}_i$ as input and finds the closest point $\mathbf{p}_k$ with respect to the measured tip pose $\mathbf{p}_m[x(t)_m, y(t)_m, \gamma(t)_m]$ from the pose sensor. Then it computes the distance error $e_d(t)$ and the orientation error $e_\theta(t)$ between $\mathbf{p}_k$ and $\mathbf{p}_m$. Combining the insertion velocity $\mathbf{u}(t)$ in the non-linear part and the orientation error $e_\theta(t)$ with the orientation gain k_θ, the path tracking controller outputs the desired angle $\theta_d(t)$ to the steering controller. On the low-level side, the PID feedback controller obtains the measured angle $\theta_m(t)$ from the curvature sensor and outputs the tension on the tendon $\mathrm{t}_c(t)$ to the plant.

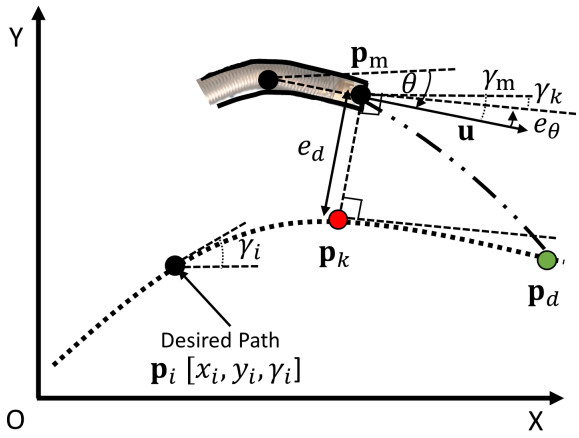

Fig. 5 Path tracking strategy: based on the current position $\mathbf{p}_m$ and the desired path $\mathbf{p}_i[x_i, y_i, \gamma_i]$, the steering angle θ can be computed by considering the distance error e_d and the orientation error e_θ with respect to the closed point $\mathbf{p}_k$ on the desired path. At the next time step, the catheter will intersect with the path on point $\mathbf{p}_d$ with a steady speed $\mathbf{u}$.

According to the bicycle model [34], the time derivative of the distance error, $\dot{e}_d(t)$, can be written as follows:

$$\dot{e}_d(t) = -\|\mathbf{u}(t)\| \sin\left(\arctan\left(\frac{k_d e_d(t)}{\|\mathbf{u}(t)\|}\right)\right) = \frac{-k_d e_d(t)}{\sqrt{1+\left(\frac{k_d e_d(t)}{\|\mathbf{u}(t)\|}\right)^2}} \tag{4}$$

and hence, for a small distance error e_d,

$$e_d(t) \approx e_d(0)\, exp - k_d t \tag{5}$$

Thus, the distance error converges exponentially to zero.

3.2.2 Low-level (feedback) controller

The desired steering angle is then sent to the low-level controller, which is a PID feedback controller in the actuation space (eq. (6)).

$$t_C(t) = K_p \cdot e(t) + K_i \cdot dt \sum_{i=0}^{t} e(t) + K_d \frac{e(t) - e(t-1)}{dt} \tag{6}$$

where $t_C(t)$ is the tension applied on the tendon, $e(t)$ is the error between the desired steering angle, $\theta_d(t)$, and the measured steering angle, $\theta_m(t)$, and K_p, K_i, K_d are the proportional, integral and derivative gains, respectively.

4 Experimental Setup and Protocols

4.1 Experimental Setup

The experiment was performed by actuating and controlling a tendon-driven steerable catheter using a sleeve-based robotic catheter driver. Moreover, a 6-DOFs EM sensor (NDI, Canada) was attached to the tip of the steerable catheter as the pose sensor, and an FBG stylet (FBGS, Technologies GmbH. Germany) with 1 cm spacing was placed in the channel of the catheter as the curvature sensor (Fig. 6). All the data communication was conducted and synchronized on the ROS (Robot Operating System).

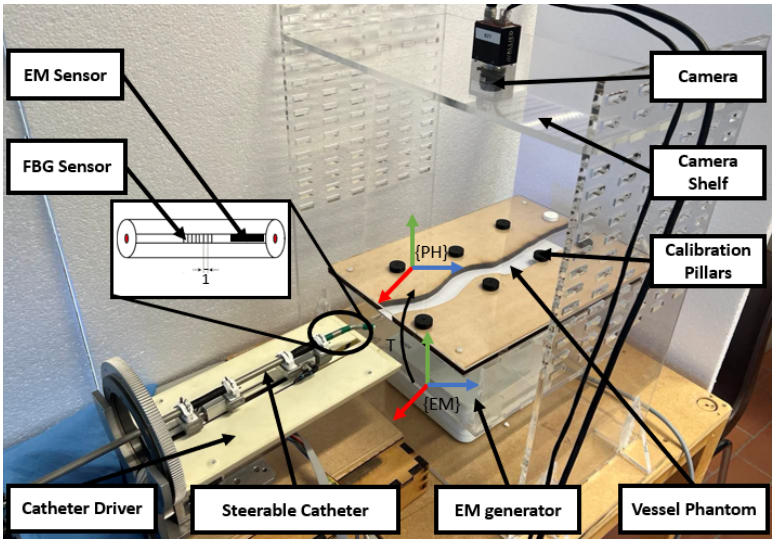

Fig. 6 Experimental setup: A tendon-driven steerable catheter, equipped with an EM sensor and a FBG style of 1 cm spacing. The catheter drive advances the steerable catheter into the vessel phantom, which is placed on top of the EM generator. In addition, eight calibration pillars are used to find the transformation matrix **T**, between the EM reference frame {**EM**}, and the phantom reference frame {**PH**}. A camera is mounted above to record the trajectory as the ground truth.

The EM generator was placed below the catheter to generate the magnetic field for tracking the EM sensor, which acquires the pose at 40 Hz with a standard deviation of 1.4 mm, A calibration procedure was implemented to compute the registration matrix between the vessel phantom and the EM coordinate. The position of eight calibration pillars was measured, which were pre-set on the phantom with a 6-DOFs EM probe (NDI, Canada). Each position was acquired ten times to reduce the acquisition error and reject the noise from the EM sensor. Then the transformation matrix, **T**, between the pillar's positions in phantom space {**PH**} and the pillar position in the EM space {**EM**} was calculated based on the singular value decomposition approach [35].

The wavelengths from the FBG interrogator Were obtained (FBGS, Technologies GmbH. Germany) and converted to a point cloud depicting the shape of the catheter

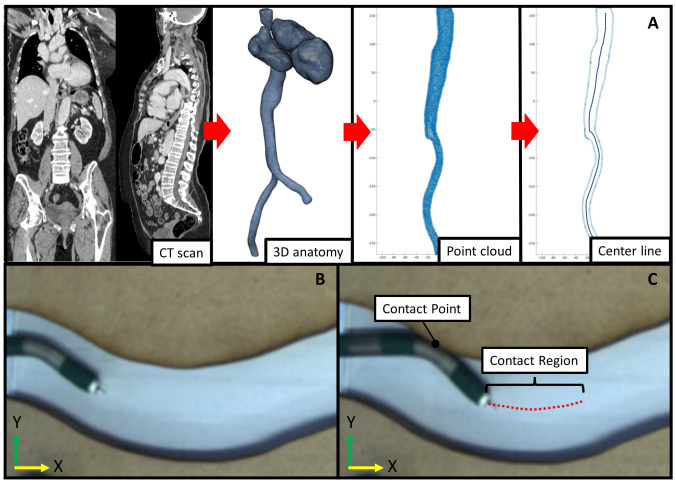

Fig. 7 (A) Extracting patient-specific test path; (B) The steerable catheter works in free space; (C) The catheter body collides with the upper boundary of the vessel phantom starting at the contact point and the navigation continues in the contact region with the constraint.

[36]. To measure the steering angle, two points were selected at the distal end of the FBG stylet to represent the orientation of the tip and two points behind to represent the orientation of the base. Those last two points were selected by calibrating the steering angle with a protractor.

Based on the Computed tomography (CT) scan images that we obtained from the hospital (Ospedale San Raffaele, Milan, Italy), the 3D anatomical model of the vessel was manually segmented and reconstructed using 3D slicer (Harvard University, National Institutes of Health). Then, the 3D anatomy was projected in the coronal plane, similar to the fluoroscopy image in the clinical procedure, and obtained the 2D point cloud of the vessel boundary in Matlab (Mathworks, Massachusetts, United States). The center line Was extracted from the boundary of the vessel as the desired path (Fig. 7, (A)). The vessel phantom had the laser cutting boundary for the shape of the vessel and two acrylic planes for constraining motion in a plane. To reduce the friction resulting from the radial compression of the wooden boundary against the catheter body, a scaling factor of 1.5 to the vessel phantom was applied. The experiment was carried out in the first 60mm section of the vessel phantom, which is the projection of the femoral vein and the iliac vein and the most tortuous part.

To measure and evaluate the accuracy of the proposed approach, a camera (Prosilica GT, Allied Vision Technologies GmbH. Germany) with a resolution of 31 megapixels and frame rates of 53 frames per second was mounted on a shelf above the phantom to record the trajectory of the catheter as the ground truth. One piece of green tape was attached to the tip of the catheter as the tracking markers. Before each test, a checkboard with 25×25 mm squares was put below the camera for calibration. The camera data was processed by converting the unit from pixel to millimeter based on the calibration data.

4.2 Experimental Protocols

To evaluate the accuracy of the control framework at each measured point j, we calculated the tracking error, e_j, which was the minimum Euclidean distance between the measured tip position of the catheter $\mathbf{p}_j(x_j, y_j)$ from the camera data and the pre-defined desired path $\mathbf{p}_i(x_i, y_i)$, which contains I points (eq. 7).

$$e_j = \min_{i,i\in\{1,2,\ldots,I\}} \|\mathbf{p}_j - \mathbf{p}_i\| = \min_{i,i\in\{1,2,\ldots,I\}} \sqrt{(x_j - x_i)^2 + (y_j - y_i)^2} \tag{7}$$

However, the distribution of errors along the entire path is not normal, because the level of challenge in navigating the catheter under various environmental constraints is different due to the insertion speed $\mathbf{u}$, and the path geometry. To comprehensively evaluate tracking accuracy throughout the entire path, all the measurement was divided into ten equal sections, which contain n measured points. The associated median value (MED) in each section was calculated, which allowed us to intuitively compare the performance of the controller under different settings. Matlab (Mathworks, United States) was also used to calculate the maximum value (Max), and Interquartile range (IQR), and perform chi-squared statistical analyses ($p < 0.05$). In total, eight tests were carried out, and the velocity dependency was analyzed by setting the insertion speed $\mathbf{u}$ at 1 mm/s, 2mm/s, and 3 mm/s.

The proposed autonomous control framework was compared with a hybrid control system, which used a joystick controller (PS4, SONY Inc.) as the control element. In this system, the experiment participant was asked to maintain the tip of the catheter at the center of the vessel by controlling the steering DOF of the catheter with the joystick, while the catheter driver autonomously progressed the catheter at a constant insertion speed of 1 mm/s. After three tests, the most confident trajectory was selected as the hybrid control group to compare with the proposed autonomous control framework.

The controller was validated in both a free space and a constrained environment. In the first half of the path, there is no contact between the catheter and the boundary of the phantom (Fig. 7 (B)). Then the catheter body collided with the upper boundary but navigation continues (Fig. 7 (C)). The MED, Max, IQR was computed to evaluate the tracking accuracy in the region with and without environmental constraints.

5 Experimental Results and Discussion

5.1 Results

With the proposed controller, the tip of the robotic catheter successfully follows the center line of the vessel phantom. Fig. 8 (A $\sim$ H) presents the trajectories recorded by the camera corresponding with different insertion speed and control gains, in which the real trajectories of the catheter tip in blue follow the centerline in red, and away from the black vessel border. The p-value of the chi-squared test show that the insertion speed is significantly affecting the tracking performance. The tracking results in the box plots indicate that the increase in the insertion speed will raise the tracking error because the robot doesn't have enough time to respond and converge to the desired path. When the catheter is inserted at 1 mm/s, the controller has the most accurate

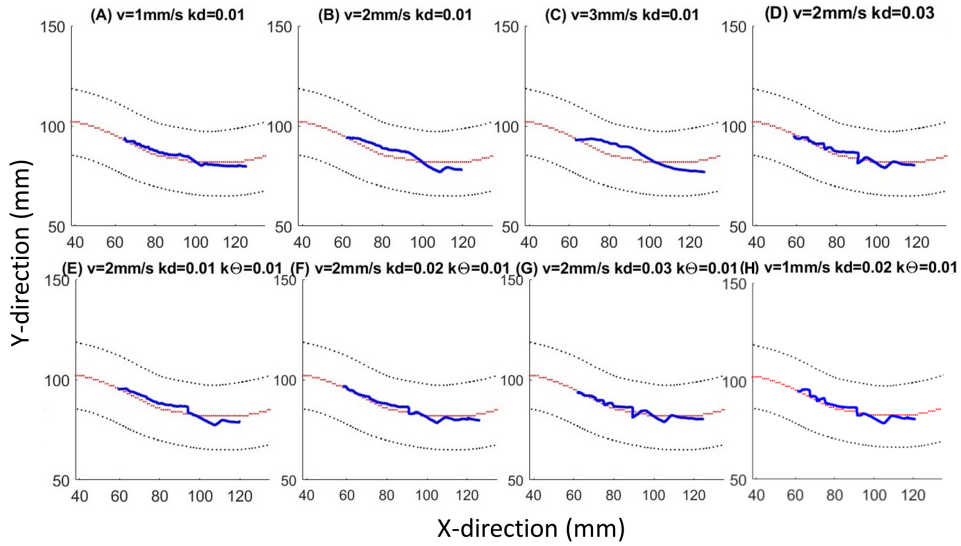

Fig. 8 Results of the path tracking experiment: (A $\sim$ H) Plots depict the tracking results with different settings, where the black lines represent the boundary of the vessel, the red lines represent the centerline of the vessel, and the blue lines are the recorded real trajectory from the camera data.

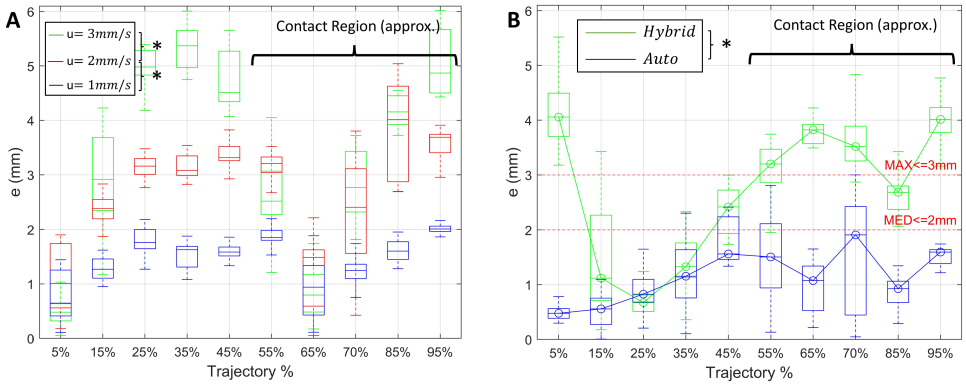

Fig. 9 Experimental results in the box plots: (A) Experimental results show the performance of the controller at a different speed u in the range of 1 mm/s to 3 mm/s; (B) Tracking errors of the hybrid control method in green and the path tracking control in blue; $*$: p-value < 0.001.

performance with a MED along the entire path of 1.43 mm, and a Max of 2.19 mm (Fig 9 (A)). Compared with the hybrid control system, which has a MED value of 2.65 mm and a Max of 5.51 mm, the result in group G with the optimal control gain has a median value below 2 mm and a maximum error below 3 mm (Fig. 9 (B)).

The contact between the catheter body and the vessel wall was identified at approximately 50% of the trajectory where a salient drop was observed. To show the precision of the controller in both free space and the contact region, the MED, Max, and IQR in those regions were calculated and compared (Table 1). No significant difference was

identified with the chi-squared test, indicating that the controller performed consistently in both free space and contact regions, across different insertion speeds regarding Group H, G, and C.

Table 1 Performance comparison in free space and in contact region regarding the insertion speed

	Free space (mm)			Contact region (mm)		
$\|\mathbf{u}\|$ (mm/s)	MED	Max	IQR	MED	Max	IQR
1	1.07	2.10	0.68	1.53	2.20	0.67
2	1.35	2.42	0.65	0,91	3.00	0.83
3	3.43	6.00	1.67	3.46	6.01	2.92

5.2 Discussion

We proposed a control framework to allow a safer and more autonomous insertion by avoiding contact between the catheter tip and the vessel wall. Our method achieves a convincing result and the insertion velocity has been considered in the control loop. In cardiovascular applications, the required precision that clinicians indicate as being acceptable is typically in the order of $1-3$ mm [37, 38]. Our results from the in-vitro studies showed that fidelity of the tracking could satisfy this requirement. Note that the test path does not cover the entire vessel which is 330 mm, because of the limited length of the catheter. A shortcoming of this work is the lack of adaptive methodology for regulating the insertion speed and the control gain factors. The insertion speed affects the performance of the controller and the final procedure time. The control gain factors are sensitive to the radius of the path and the contact region. Given these same wrenches, a Bayesian optimization approach may be used to choose those parameters for the patient-specific path.

In the future, the proposed controller can be extended in these two directions. 1) Path tracking with 3-D path: combing the rotation of the working plane could allow the catheter to achieve any points in the cartesian space. Furthermore, the working plane should be properly chosen to compensate for the gravity effect. 2) Adaptive control: The insertion velocity and the control gain factors could be regulated automatically based on the Bayesian optimization method to self-adapt different paths, which can reduce tracking errors and minimize the procedure time.

6 Conclusion

In this work, we proved the feasibility of controlling a robotic catheter to track a given path with the proposed control framework. A tendon-driven steerable catheter was actuated and tested in vitro. The results suggest the potential for increasing the level of autonomy in robotic catheters to revolutionize transcatheter cardiology interventions. Compared with other model-based or model-less feedback control methods, our method achieves satisfying accuracy without the request of calibrating the intuitive

parameters nor acquiring a training dataset. Moreover, nonholonomic motion planning and control have been extensively explored in robotics literature, allowing us to leverage a vast array of existing research in applying our model.

Acknowledgments. The authors would like to thank Madhan Chirumamilla from FBGS Technologies GmbH. for providing the sensors and the RAS group at KU Leuven for their suggestions on the experimental setup.

Declarations

- **Conflict of interest** The authors have no relevant financial or nonfinancial interests to disclose.
- **Funding** This work was supported by the European Union's Horizon 2020 research and innovation program, under the project ARTERY, grant agreement No. 101017140.

References

[1] Mirabel, M., Iung, B., Baron, G., Messika-Zeitoun, D., Détaint, D., Vanoverschelde, J.-L., Butchart, E.G., Ravaud, P., Vahanian, A.: What are the characteristics of patients with severe, symptomatic, mitral regurgitation who are denied surgery? European heart journal **28**(11), 1358–1365 (2007)

[2] Zhang, X., Palumbo, M.C., Perico, F., Magro, M., Fortuna, A., Magni, T., Votta, E., Segato, A., De Momi, E.: Robotic actuation and control of a catheter for structural intervention cardiology. In: 2022 IEEE/RSJ International Conference on Intelligent Robots and Systems (IROS), pp. 5907–5913 (2022). IEEE

[3] Li, Z., Dankelman, J., De Momi, E.: Path planning for endovascular catheterization under curvature constraints via two-phase searching approach. International Journal of Computer Assisted Radiology and Surgery **16**, 619–627 (2021)

[4] Chhatriwalla, A.K., Vemulapalli, S., Holmes, D.R.J., Dai, D., Li, Z., Ailawadi, G., Glower, D., Kar, S., Mack, M.J., Rymer, J., Kosinski, A.S., Sorajja, P.: Institutional experience with transcatheter mitral valve repair and clinical outcomes: Insights from the tvt registry. JACC Cardiovascular Interventions **12(14)**, 1342–1352 (2019)

[5] Granada, J.F., Delgado, J.A., Uribe, M.P., Fernandez, A., Blanco, G., Leon, M.B., Weisz, G.: First-in-human evaluation of a novel robotic-assisted coronary angioplasty system. JACC: Cardiovascular Interventions **4**(4), 460–465 (2011)

[6] Rillig, A., Schmidt, B., Di Biase, L., Lin, T., Scholz, L., Heeger, C.H., Metzner, A., Steven, D., Wohlmuth, P., Willems, S., Trivedi, C., Galllinghouse, J.G., Natale, A., Ouyang, F., Kuck, K.-H., Tilz, R.R.: Manual versus robotic catheter ablation for the treatment of atrial fibrillation: the man and machine trial. JACC: Clinical Electrophysiology **3**(8), 875–883 (2017)

[7] Valderrábano, M., Dave, A.S., Báez-Escudero, J.L., Rami, T.: Robotic catheter ablation of left ventricular tachycardia: initial experience. Heart Rhythm **8**(12), 1837–1846 (2011)

[8] Bassil, G., Markowitz, S.M., Liu, C.F., Thomas, G., Ip, J.E., Lerman, B.B., Cheung, J.W.: Robotics for catheter ablation of cardiac arrhythmias: Current technologies and practical approaches. Journal of Cardiovascular Electrophysiology **31**(3), 739–752 (2020)

[9] Shi, P., Guo, S., Zhang, L., Jin, X., Hirata, H., Tamiya, T., Kawanishi, M.: Design and evaluation of a haptic robot-assisted catheter operating system with collision protection function. IEEE Sensors Journal **21**(18), 20807–20816 (2021)

[10] Woo, J., Song, H.-S., Cha, H.-J., Yi, B.-J.: Advantage of steerable catheter and haptic feedback for a 5-dof vascular intervention robot system. Applied Sciences **9**(20), 4305 (2019)

[11] Zhang, L., Guo, S., Yu, H., Song, Y., Tamiya, T., Hirata, H., Ishihara, H.: Design and performance evaluation of collision protection-based safety operation for a haptic robot-assisted catheter operating system. Biomedical microdevices **20**(2), 1–14 (2018)

[12] Dupont, P.E., Nelson, B.J., Goldfarb, M., Hannaford, B., Menciassi, A., O'Malley, M.K., Simaan, N., Valdastri, P., Yang, G.-Z.: A decade retrospective of medical robotics research from 2010 to 2020. Science Robotics **6**(60), 8017 (2021)

[13] Yang, G.-Z., Cambias, J., Cleary, K., Daimler, E., Drake, J., Dupont, P.E., Hata, N., Kazanzides, P., Martel, S., Patel, R.V., Santos, V.J., Taylor, R.H.: Medical robotics—Regulatory, ethical, and legal considerations for increasing levels of autonomy. American Association for the Advancement of Science (2017)

[14] Jolaei, M., Hooshiar, A., Dargahi, J., Packirisamy, M.: Toward task autonomy in robotic cardiac ablation: Learning-based kinematic control of soft tendon-driven catheters. Soft Robotics **8**(3), 340–351 (2021)

[15] Yip, M.C., Sganga, J.A., Camarillo, D.B.: Autonomous control of continuum robot manipulators for complex cardiac ablation tasks. Journal of Medical Robotics Research **2**(01), 1750002 (2017)

[16] Slawinski, P.R., Simaan, N., Obstein, K.L., Valdastri, P.: Sensorless estimation of the planar distal shape of a tip-actuated endoscope. IEEE robotics and automation letters **4**(4), 3371–3377 (2019)

[17] Ganji, Y., Janabi-Sharifi, F.: Catheter kinematics for intracardiac navigation. IEEE Transactions on Biomedical Engineering **56**(3), 621–632 (2009)

[18] Greigarn, T., Poirot, N.L., Xu, X., Çavuşoğlu, M.C.: Jacobian-based task-space motion planning for mri-actuated continuum robots. IEEE robotics and automation letters **4**(1), 145–152 (2018)

[19] Rucker, D.C., Webster, R.J.: Computing jacobians and compliance matrices for externally loaded continuum robots. In: 2011 IEEE International Conference on Robotics and Automation, pp. 945–950 (2011). IEEE

[20] Greigarn, T., Jackson, R., Liu, T., Çavuşoğlu, M.C.: Experimental validation of the pseudo-rigid-body model of the mri-actuated catheter. In: 2017 IEEE International Conference on Robotics and Automation (ICRA), pp. 3600–3605 (2017). IEEE

[21] Bailly, Y., Amirat, Y., Fried, G.: Modeling and control of a continuum style microrobot for endovascular surgery. IEEE Transactions on Robotics **27**(5), 1024–1030 (2011)

[22] Coevoet, E., Escande, A., Duriez, C.: Optimization-based inverse model of soft robots with contact handling. IEEE Robotics and Automation Letters **2**(3), 1413–1419 (2017)

[23] Yip, M.C., Camarillo, D.B.: Model-less feedback control of continuum manipulators in constrained environments. IEEE Transactions on Robotics **30**(4), 880–889 (2014)

[24] Wu, D., Ha, X.T., Zhang, Y., Ourak, M., Borghesan, G., Niu, K., Trauzettel, F., Dankelman, J., Menciassi, A., Vander Poorten, E.: Deep-learning-based compliant motion control of a pneumatically-driven robotic catheter. IEEE Robotics and Automation Letters **7**(4), 8853–8860 (2022)

[25] Chikhaoui, M.T., Burgner-Kahrs, J.: Control of continuum robots for medical applications: State of the art. In: ACTUATOR 2018; 16th International Conference on New Actuators, pp. 1–11 (2018). VDE

[26] Shi, C., Luo, X., Qi, P., Li, T., Song, S., Najdovski, Z., Fukuda, T., Ren, H.: Shape sensing techniques for continuum robots in minimally invasive surgery: A survey. IEEE Transactions on Biomedical Engineering **64**(8), 1665–1678 (2016)

[27] Dore, A., Smoljkic, G., Vander Poorten, E., Sette, M., Vander Sloten, J., Yang, G.-Z.: Catheter navigation based on probabilistic fusion of electromagnetic tracking and physically-based simulation. In: 2012 IEEE/RSJ International Conference on Intelligent Robots and Systems, pp. 3806–3811 (2012). IEEE

[28] Loschak, P.M., Brattain, L.J., Howe, R.D.: Algorithms for automatically pointing ultrasound imaging catheters. IEEE Transactions on Robotics **33**(1), 81–91 (2016)

[29] Omisore, O.M., Han, S.P., Ren, L.X., Wang, G.S., Ou, F.L., Li, H., Wang, L.: Towards characterization and adaptive compensation of backlash in a novel robotic catheter system for cardiovascular interventions. IEEE transactions on biomedical circuits and systems **12**(4), 824–838 (2018)

[30] Sefati, S., Murphy, R.J., Alambeigi, F., Pozin, M., Iordachita, I., Taylor, R.H., Armand, M.: Fbg-based control of a continuum manipulator interacting with obstacles. In: 2018 IEEE/RSJ International Conference on Intelligent Robots and Systems (IROS), pp. 6477–6483 (2018). IEEE

[31] Al-Ahmad, O., Ourak, M., Smits, J., Jeanquart, S., Deserranno, N., Bernhard, F., Kassahun, Y., Yu, B., Vander Poorten, E.: Development of an innovative sleeve-based robotic catheter driver. In: Joint Workshop on New Technologies for Computer/Robot Assisted Surgery, Date: 2018/09/10-2018/09/11, Location: London (2018)

[32] Webster III, R.J., Kim, J.S., Cowan, N.J., Chirikjian, G.S., Okamura, A.M.: Nonholonomic modeling of needle steering. The International Journal of Robotics Research **25**(5-6), 509–525 (2006)

[33] Thrun, S., Montemerlo, M., Dahlkamp, H., Stavens, D., Aron, A., Diebel, J., Fong, P., Gale, J., Halpenny, M., Hoffmann, G., Lau, K., Oakley, C., Palatucci, M., Pratt, V., Stang, P.: Stanley: The robot that won the darpa grand challenge. Journal of field Robotics **23**(9), 661–692 (2006)

[34] Fallahi, B., Khadem, M., Rossa, C., Sloboda, R., Usmani, N., Tavakoli, M.: Extended bicycle model for needle steering in soft tissue. In: 2015 IEEE/RSJ International Conference on Intelligent Robots and Systems (IROS), pp. 4375–4380 (2015). IEEE

[35] Boles, M., Fu, J., Iovene, E., Francesco, C., Ferrigno, G., De Momi, E.: Augmented reality and robotic navigation system for spinal surgery. In: Proceeding of the 11th Joint Workshop on New Technologies for Computer/Robot Assisted Surgery, pp. 96–97 (2022)

[36] Al-Ahmad, O., Ourak, M., Van Roosbroeck, J., Vlekken, J., Vander Poorten, E.: Improved fbg-based shape sensing methods for vascular catheterization treatment. IEEE Robotics and Automation Letters **5**(3), 4687–4694 (2020)

[37] Nijland, H., Gerbers, J., Bulstra, S., Overbosch, J., Stevens, M., Jutte, P.: Evaluation of accuracy and precision of ct-guidance in radiofrequency ablation for osteoid osteoma in 86 patients. PLoS One **12**(4), 0169171 (2017)

[38] Bourier, F., Reents, T., AMMAR-BUSCH, S., Buiatti, A., Grebmer, C., Telishevska, M., Brkic, A., Semmler, V., Lennerz, C., Kaess, B., Kottmaier, M., Kolb, C., Deisenhofer, I., Hessling, G.: Sensor-based electromagnetic navigation (mediguide®): How accurate is it? a phantom model study. Journal of

cardiovascular electrophysiology **26**(10), 1140–1145 (2015)